Exceptionally Strong Phonon Scattering by B Substitution in Cubic SiC

Ankita Katre,[1,*] Jesús Carrete,[2] Bonny Dongre,[2] Georg K. H. Madsen,[2] and Natalio Mingo[1,†]

[1]*LITEN, CEA-Grenoble, 17 rue des Martyrs, 38054 Grenoble Cedex 9, France*
[2]*Institute of Materials Chemistry, TU Wien, A-1060 Vienna, Austria*

We use *ab initio* calculations to predict the thermal conductivity of cubic SiC with different types of defects. An excellent quantitative agreement with previous experimental measurements is found. The results unveil that B_C substitution has a much stronger effect than any of the other defect types in 3*C*-SiC, including vacancies. This finding contradicts the prediction of the classical mass-difference model of impurity scattering, according to which the effects of B_C and N_C would be similar and much smaller than that of the C vacancy. The strikingly different behavior of the B_C defect arises from a unique pattern of resonant phonon scattering caused by the broken structural symmetry around the B impurity.

Silicon carbide (SiC) plays a fundamental role in many emerging technologies, ranging from biomedical sensors to optoelectronics, power electronics, and photovoltaics [1–9]. Most notably, this material has been termed the "linchpin to green energy" that may replace Si-based technology in power electronics [1], owing partly to its large lattice thermal conductivity κ. From the many stable polytypes of SiC [10], two of the hexagonal ones, 6*H*-SiC and 4*H*-SiC, have been extensively studied and widely used [10–12]. In contrast, the structurally less complex cubic polytype of SiC with the zinc-blende structure (3*C*-SiC) is much less well understood, despite presumably having the best electronic properties [13], and, as we will see, possibly a higher κ than the other polytypes. This is partly due to the difficulty in synthesizing high quality crystals, although recent improvements in 3*C*-SiC growth techniques have prompted a renewed interest in it [13].

Surprisingly, the reference measurements of κ on pure undoped 3*C*-SiC are over 20 years old and little detail is known about the quality of the samples [10,14]. The reference value of κ for the 3*C* phase is perplexingly lower than that for the structurally more complex 6*H* phase, raising doubts about whether this is truly an intrinsic property or just a consequence of the defective, polycrystalline quality of the 3*C*-SiC samples. A very recent study [15] has shown that structural complexity and thermal conductivity are inversely correlated in the series of hexagonal phases of SiC, contrary to historical measurements, which could be afflicted with similar problems [10,14]. It is then clear that to understand the conduction properties of 3*C*-SiC, and to harness its full potential, one must first comprehend the way defects affect it. As we show here, by comparing predictive *ab initio* calculations with experiments on defective samples, a richer physical picture emerges, unveiling striking differences in the way different dopants affect κ. It also indirectly suggests that the intrinsic κ of defect-free 3*C*-SiC should be much

higher than previously reported and surpass that of the 6*H* phase.

In this Letter, we compare our theoretical results to the measured $\kappa(T)$ curves for doped samples of 3*C*-SiC [16]. We use an *ab initio* approach to quantify the phonon scattering rates of N_C substitutional defects. The predicted κ is in excellent agreement with the experimental results. This then allows us to explain the effect of codoping with N and B, and shows that B impurities scatter phonons 2 orders of magnitude more strongly overall than N or Al impurities, and as strongly as C vacancies. We identify resonant phonon scattering as the reason for this behavior, resulting from distortion and broken symmetry around the B atom. We then show this resonant scattering behavior to be a general phenomenon that can take place for strong enough perturbations.

κ for cubic structures can be obtained from a complete phonon picture as explained in Refs. [17,18]. We use an iterative scheme to solve the full linearized Boltzmann transport equation (BTE) and calculate κ of 3*C*-SiC as implemented in the ALMABTE code [19]. Details about the calculations are presented in the Supplemental Material [20], which includes Refs. [17–19,21–30].

The calculated κ for defect-free single-crystal 3*C*-SiC is shown as the brown dashed line in Fig. 1 and is in good agreement with earlier calculations [31]. The value of κ at 300 K is 552 W/m K, which is about ∼70% higher than the experimentally reported κ (320 W/m K) [14,32]. It also surpasses the experimental κ at 300 K for the 6*H*-SiC phase by ∼10% [32]. Inclusion of Si and C isotope scattering slightly lowers the calculated κ (orange dashed line in Fig. 1), but the values remain much larger than the experimental ones.

The calculated κ for the defective structures of 3*C*-SiC are compared with experiments on polycrystalline samples from Ref. [16] in Fig. 1. The additional contribution of the grain boundaries to the scattering rate is included in the standard way as $\tau_{j\mathbf{q},\mathrm{grain}}^{-1} = |v_{j\mathbf{q}}|/L_{\mathrm{grain}}$, where $|v_{j\mathbf{q}}|$ is the norm of the
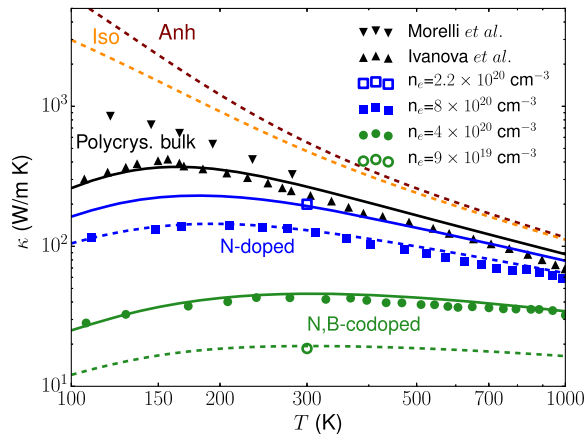
FIG. 1.   Calculated κ of 3C-SiC including, progressively, anharmonic phonon scattering, isotope scattering, grain boundary scattering (--- $L_{\text{grain}} = 0.8$ μm), and different concentrations of defects [--- 2.2×10^{20} cm^{-3} N$_C$ (0.45%), -- -- 8×10^{20} cm^{-3} N$_C$ (1.63%), --- 6.6×10^{20} cm^{-3} N$_C$ (1.3%), 2.6×10^{20} cm^{-3} B$_C$ (0.5%), and -- -- 1.32×10^{21} cm^{-3} N$_C$ (2.7%), 1.23×10^{21} cm^{-3} B$_C$ (2.5%)]. The experiments are from Morelli et $al.$ [14] and Ivanova et $al.$ [16].

FIG. 2.   3C-SiC κ variation with defect concentration for Al$_{\text{Si}}$, N$_C$, Vac$_C$, and B$_C$ defects. The low value of κ associated with the B$_C$ defect is related to its anisotropic lattice relaxation seen in the inset (and in the Supplemental Material [20]). The changes in the nearest-neighbour interatomic distances are directly proportional to the bond-width variations shown in the inset.

phonon group velocity vector for a phonon mode $j\mathbf{q}$ (j represents the phonon branch and $\mathbf{q}$ the wave vector) and L_{grain} is the grain size. Employing $L_{\text{grain}} = 0.8$ μm for all the samples yields good agreement with experiment.

The black filled triangles in Fig. 1 are the experimental measurements on the polycrystalline bulk sample without any dopant [16]. The other experimental results are for the N-doped, and N- and B-codoped n-type samples in Ref. [16]. The case of N-only doping demonstrates the predictive power of the ab $initio$ approach. As N in SiC can be considered as a shallow donor [33–35] and each dopant contributes one electron per defect atom, the concentrations of N$_C$ defects can be expected to be the same as the carrier concentration. Using the carrier concentrations for different N-doped 3C-SiC samples reported in Ref. [16] yields excellent agreement between the calculated and the experimental κ for the whole temperature range in Fig. 1 (blue lines and symbols). This confirms the reliability of the ab $initio$ approach.

The case of B and N codoping is considered next. B substitutes for C in 3C-SiC when it is grown in Si-rich conditions [36–38]. The fact that the undoped samples in Ref. [16] are n type with a reasonably high carrier concentration ($\approx 10^{17}$ cm^{-3}) would indicate the formation of vacancies at C sites and in turn Si-rich growth conditions [39]. Because of codoping, the carrier concentrations given in Ref. [16] correspond to the difference between the donor and acceptor concentrations, and thus they do not uniquely determine the defect densities. In this case, we determine the individual defect densities by keeping the difference in concentrations equal to the experimental carrier concentration. The calculation matches the whole
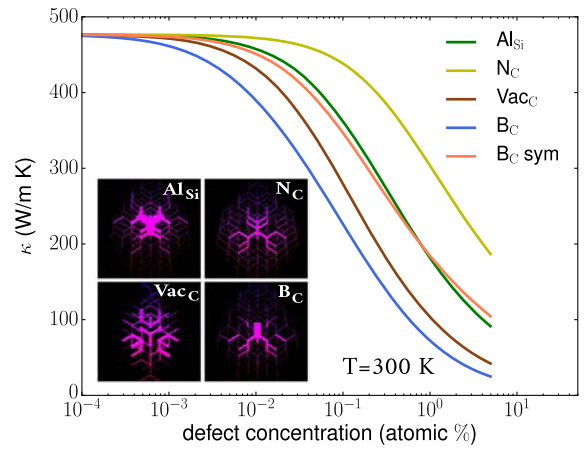
temperature dependent experimental curve only if the individual concentrations are 1.3% and 0.5% for N$_C$ and B$_C$, respectively (Fig. 1, upper green line and circles). The relative concentrations of the other codoped sample were similarly derived yielding 2.7% and 2.5% of N$_C$ and B$_C$ defects, respectively (lower green line and circle in Fig. 1). Our calculations capture the correct experimental trend of a big reduction in κ seen when B$_C$ defects, even in smaller concentrations than N$_C$, are introduced in the samples (Fig. 1). This evidences the much stronger phonon scattering strength induced by B$_C$ defects. Furthermore, Fig. 2 shows the dependence of κ on impurity concentration, and confirms the anomalously large scattering from B$_C$ defects. This behavior of the B$_C$ defects seems the only possible explanation of the very low κ (42 and 19 W/m K at 300 K) measured for the codoped samples. Otherwise, to achieve the same low thermal conductivities by N doping alone would require the N$_C$ concentrations in excess of 20%, which are obviously unrealistic.

A look at the phonon scattering rates in Fig. 3(b) provides more clues about boron's atypical behavior. Scattering by substitutional impurities comes from two sources: the mass difference between the impurity atom and the one it replaces, and the local change in the interatomic force constants (IFCs) around the impurity in response to structural relaxation and a modified chemical environment. In cases like Ge impurities in Si, the mass term dominates because Si and Ge have similar chemical bonding properties but very different masses [40,41]. The other extreme is the case of vacancies, where the host atom is absent and the only contribution comes from IFC differences. The B-induced scattering rates in Fig. 3(b) are a striking 2 orders of magnitude larger than the N-induced ones, and they are comparable to those of the C vacancy. This is
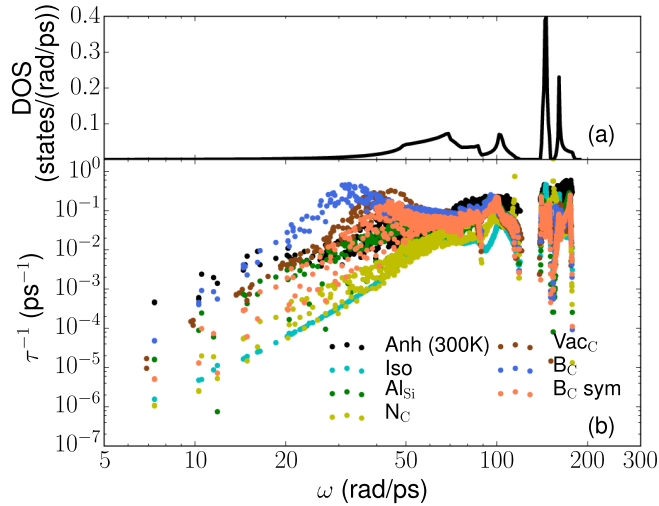
FIG. 3.   (a) Phonon DOS of SiC and (b) scattering rates of phonons by different defects (with a concentration of 10^{20} cm^{-3}), isotopes, and phonon-phonon interactions at 300 K.

surprising because the absolute value of the mass difference between B and C is nearly the same as between N and C. A calculation including only mass differences, and neglecting IFC differences does indeed predict very similar scattering rates for B and N impurities (see Fig. S1 of the Supplemental Material [20]). Therefore, the large scattering rates for B must come from the different changes in IFCs. However, scattering by Al substitutionals is not nearly as large as that of B, despite both species belonging to the same column in the periodic table, which might lead one to expect similar chemical bonding properties.

Figure 4 shows the norm of the changes in the on-site IFC submatrices. Since translation symmetry imposes a set
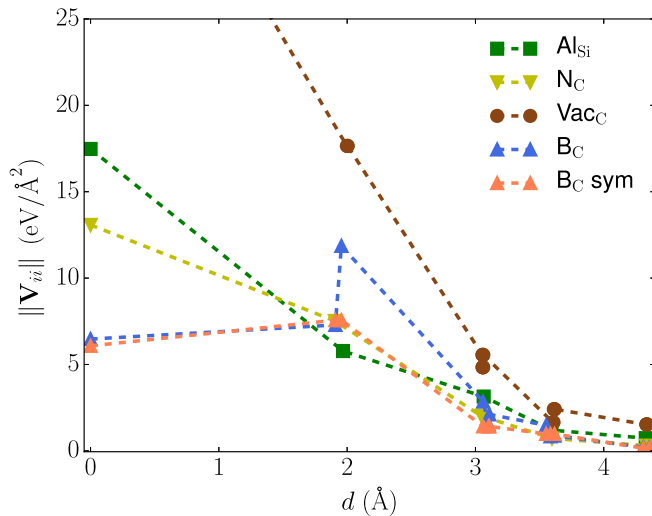

FIG. 4.   Frobenius norm of the changes in the on-site IFC submatrices of the atoms (i) around the defects with respect to the perfect 3C-SiC structure as a function of the distance of the atoms from the defect center (d).

of linear constraints on each row of the IFC matrix, the change in the on-site terms probes the overall change in the IFCs related to each atom. The results shown in the figure confirm that the largest changes happen in the case of the vacancy. On the other hand, the B_C defect shows a rather large asymmetry in the first-neighbor shell, which may explain the increased scattering. To be able to analyze the contribution to scattering from this asymmetry, we define a symmetric perturbation matrix $\mathbf{V}_{sym}$ containing only the part of the total perturbation matrix $\mathbf{V}$ (see details in the Supplemental Material [20]) calculated by averaging $\mathbf{V}$ over the four space-group operations that just permute the four nearest neighbors of the defect center. Hence, $\mathbf{V}$ can be split as a sum of this symmetric term plus an asymmetric term containing the remainder of the total perturbation: $\mathbf{V} = \mathbf{V}_{sym} + \mathbf{V}_{asym}$. Figures 2 and 3 show the variation of κ with defect concentration and the phonon-defect scattering rates induced by the artificial defect represented by $\mathbf{V}_{sym}$. Likewise, the norm of the changes in the on-site IFC submatrices due to $\mathbf{V}_{sym}$ is shown in Fig. 4. It can be seen that the symmetrization process does indeed bring the values more in line with those corresponding to the symmetric perturbations N_C and Al_{Si}. Accordingly, the symmetrized B_C perturbation yields thermal conductivities very similar to those from Al_{Si} impurities, and much larger than those for the same concentration of true B_C impurities, as shown in Fig. 2.

The asymmetry in IFCs is caused by an asymmetry in the relaxed structure of the B_C defect. While both N and Al lead to relaxations around the impurity maintaining tetrahedral (T_d) symmetry, the relaxation around B breaks the symmetry and the impurity gets closer to three of its four nearest neighbors showing threefold (C_{3v}) symmetry [Fig. 2 (inset); see also Ref. [38]]. The asymmetrical relaxed structure of the B_C defect is a manifestation of the complex chemistry of boron [42]. Some insight into the different chemical behaviors of N and B with respect to Si can be gained from a look at their binary compounds. While the most stable silicon nitride is Si_3N_4, with a relatively simple structure, silicon borides have stoichiometries from SiB_3 to SiB_{40} and very complex unit cells with hundreds of atoms [43,44]. The stoichiometry and the structure of silicon borides suggest an affinity of B for low coordination with Si. Thus, the relaxation of the B defect atom away from one of its four neighboring atoms in 3C-SiC can be interpreted as a movement towards lower coordination. This type of relaxation is however not uncommon for an extrinsic defect in tetrahedral semiconductors, and can arise in the context of DX centers.

Although the above reasoning shows that symmetry breaking affects the perturbation for B_C impurities, this does not yet explain its exceptionally large effect on κ. To understand it, let us take another look at the scattering rates and the phonon density of states (DOS) of SiC in Fig. 3. The scattering rates for B_C display a prominent peak at

about 33 rad/ps. A similarly large peak is observed for the vacancy at a slightly higher frequency. Such a peak is notably smaller or almost absent for the Al_{Si} and N_C defects. The rates for the symmetrized B_C impurity are also shown (B_C sym), displaying much smaller values and a much lower peak than the original B_C perturbation. This peak is the signature of resonant scattering. Resonances are quasibound states in the continuum of propagating states. They are infinitely extended, but have a large probability around the localized perturbation that causes them. They manifest themselves as peaks in the phonon scattering cross section σ of the scatterer near the frequency of the resonance. The Green's function approach that we use to compute defect scattering rates accounts for the full scattering to all orders, so it perfectly captures the effect of resonances, which would not appear in truncated perturbative approaches.

A direct way to identify resonant scattering is via the scattering **T** matrix (see the expression in the Supplemental Material [20]), which is fundamentally related to the cross section [24,45]. Prominent peaks in the imaginary part of the trace of the scattering **T** matrix, shown in Fig. 5(a), correspond to resonances. In Fig. 5(a), these resonances are much easier to identify than from the cloud of scattering rate points in Fig. 3. The figure clearly displays large resonances for B_C and C vacancies (Vac_C), but not for the symmetrized B_C, N_C and Al_{Si}.

According to scattering theory, as the intensity of the localized perturbation grows stronger, increasingly sharper resonances start to develop at the lower frequency spectrum [46]. In the present case, this would imply that resonances might show up for impurities other than B_C or C vacancies, if only their perturbations were stronger. To verify this, we have artificially multiplied the perturbation by a constant factor α, and have recalculated σ for a longitudinal-acoustic phonon of frequency 33 rad/ps (the resonant frequency for the B_C defect), as a function of α. The value $\alpha = 1$ corresponds to the true perturbation. Figure 5(b) confirms that for sufficiently large α, every impurity is able to develop resonant scattering. Figure 5(b) suggests the qualitative concept of an effective native "strength" of the defect: the B_C and C vacancy defects are associated with a larger strength, manifested as a larger cross section at small α and an earlier onset of the resonance with an increase in α. This strength is the result of a complex interplay involving the magnitude of the different changes in the IFCs and their symmetry. In the B_C case, the broken symmetry due to the T_d to C_{3v} transition leads to a visibly enhanced strength with respect to the symmetrized case, seen in Fig. 5(b), despite the overall change in the perturbation matrices in Fig. 4 not being drastic. Similar strong effects of the T_d to C_{3v} symmetry transition for extrinsic defects in tetrahedral semiconductors are also seen for charge carrier scattering [47,48].

These results have significant implications for the SiC industry. B-doped SiC has shown promising results in
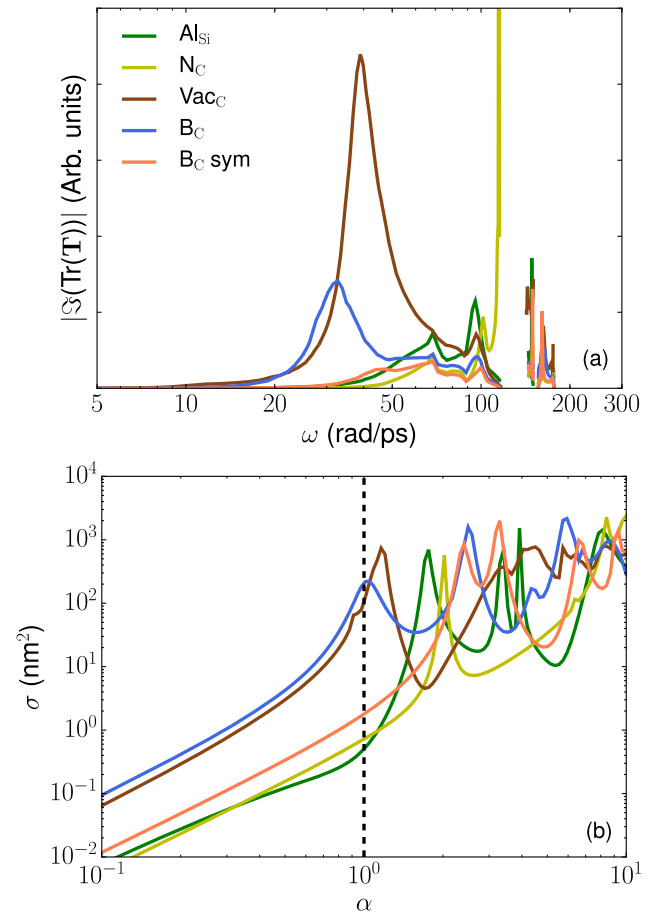

FIG. 5. (a) Trace of the imaginary part of the scattering **T** matrix for different impurities, showing a resonance for B and a vacancy. (b) Scattering cross section σ for the longitudinal-acoustic mode at an angular frequency of 33 rad/ps, as a function of scattering strength for different impurities. Similar resonance peaks for the B_C defect are also seen for transverse-acoustic phonon modes at $\sim$33 rad/ps (see Fig. S4 in the Supplemental Material [20]).

photovoltaics, power electronics, and many more applications [49–53]. However, the drastic thermal conductivity reduction associated with B doping can affect device efficiency and lifetime. Thus, balancing the improvement of electronic and luminescent properties with the detrimental effects on thermal conductivity is an important factor to consider when selecting the right dopants for these applications.

In conclusion, B_C substitutional impurities in cubic SiC scatter phonons much more strongly than N_C or Al_{Si} impurities, and comparably to C vacancies. For N impurities to reduce κ as much as B impurities do, the concentration of the former has to be roughly 30 times larger than that of the latter. This could not have been guessed from mass difference considerations. It emerges from *ab initio* calculations, which are clearly supported by previous experimental measurements. This striking behavior is caused by the symmetry transition from T_d

to C_{3v} around the B impurity upon relaxation, which leads to strong resonant scattering of acoustic phonons in the angular frequency range between 33 and 50 rad/ps. If only the symmetric part of the perturbation is kept, the resonance disappears and the calculated effect becomes similar to that of Al substitutionals, thus showing a significant impact of defect-induced symmetry breaking on the thermal conductivity of SiC. However, symmetry breaking by itself is not a sufficient condition, as seen in the case of N defects in diamond [45], where lattice distortions do not lead to resonant scattering. Furthermore, the calculations presented suggest that single-crystalline, defect-free cubic SiC can achieve a thermal conductivity about 1.7 times higher than the largest reported measured value on this polytype, and above those of other polytypes.

The results shown here point to a general phenomenon, whereby lattice distortions induced by defects showing a T_d to C_{3v} transition in different tetrahedrally bonded semiconductors [47,54] may develop into a phonon resonance and lead to enhanced scattering. This should be relevant to many rapidly evolving technologies. In complex semiconductors there will usually be several possible doping scenarios for reaching a desired carrier concentration, and the sensitivity of the phonon scattering to the specific defect thus opens up an important new route in semiconductor design.

*Corresponding author.
ankitamkatre@gmail.com
†Corresponding author.
natalio.mingo@cea.fr

[1] J. C. R. Eddy and D. K. Gaskill, Science **324**, 1398 (2009).
[2] M. Bhatnagar and B. J. Baliga, IEEE Trans. Electron Devices **40**, 645 (1993).
[3] J. Fréchette and C. Carraro, J. Am. Chem. Soc. **128**, 14774 (2006).
[4] C. Hao, X. Guo, Y. Pan, S. Chen, Z. Jiao, H. Yang, and X. Guo, J. Am. Chem. Soc. **138**, 9361 (2016).
[5] S. E. Saddow, *Silicon Carbide Biotechnology* (Elsiver, Amsterdam, 2012).
[6] R. Hillenbrand, T. Taubner, and F. Keilmann, Nature (London) **418**, 159 (2002).
[7] M. Syvajarvi, Q. Ma, V. Jokubavicius, A. Galeckas, J. Sun, X. Liu, M. Jansson, P. Wellmann, M. Linnarsson, P. Runde *et al.*, Sol. Energy Mater. Sol. Cells **145**, 104 (2016).
[8] G. Beaucarne, A. S. Brown, M. J. Keevers, R. Corkish, and M. A. Green, Prog. Photovoltaics **10**, 345 (2002).
[9] G. Cicero, A. Catellani, and G. Galli, Phys. Rev. Lett. **93**, 016102 (2004).
[10] *Properties of Silicon Carbide*, edited by G. L. Harris (ISPEC, London, 1995).
[11] N. Zheludev, Nat. Photonics **1**, 189 (2007).
[12] W. C. Lien, N. Damrongplasit, J. H. Paredes, D. G. Senesky, T. J. K. Liu, and A. P. Pisano, IEEE J. Electron Devices Soc. **2**, 164 (2014).
[13] R. Verucchi, L. Aversa, M. V. Nardi, S. Taioli, S. a Beccara, D. Alfè, L. Nasi, F. Rossi, G. Salviati, and S. Iannotta, J. Am. Chem. Soc. **134**, 17400 (2012).
[14] D. Morelli, J. Heremans, C. Beetz, W. S. Woo, G. L. Harris, and C. Taylor, Instit. Phys. Conf. Ser. **N137**, 313 (1993).
[15] N. H. Protik, A. Katre, L. Lindsay, J. Carrete, N. Mingo, and D. Broido, DOI: 10.1016/j.mtphys.2017.05.004.
[16] L. M. Ivanova, P. A. Aleksandrov, and K. D. Demakov, Inorg. Mater. (USSR) **42**, 1205 (2006).
[17] W. Li, J. Carrete, N. A. Katcho, and N. Mingo, Comput. Phys. Commun. **185**, 1747 (2014).
[18] A. Katre and G. K. H. Madsen, Phys. Rev. B **93**, 155203 (2016).
[19] J. Carrete, B. Vermeersch, A. Katre, A. Roekeghem, T. Wang, G. K. H. Madsen, and N. Mingo, Comput. Phys. Commun., DOI: 10.1016/j.cpc.2017.06.023 (2017).
[20] See Supplemental Material at http://link.aps.org/supplemental/10.1103/PhysRevLett.119.075902 for computational details, defect scattering rates considering defects as mass perturbations, anharmonic scattering rates for acoustic phonons, structural distortion of 3*C*-SiC with defects and scattering cross-section for different acoustic phonon branches with boron defect.
[21] S. I. Tamura, Phys. Rev. B **27**, 858 (1983).
[22] S. I. Tamura, Phys. Rev. B **30**, 849 (1984).
[23] N. Mingo, D. A. Stewart, D. A. Broido, L. Lindsay, and W. Li, in *Length-Scale Dependent Phonon Interactions*, edited by S. L. Shindé and G. P. Srivastava, Topics in Applied Physics No. 128 (Springer, New York, 2014), pp. 137–173.
[24] N. Mingo, K. Esfarjani, D. A. Broido, and D. A. Stewart, Phys. Rev. B **81**, 045408 (2010).
[25] P. E. Blöchl, Phys. Rev. B **50**, 17953 (1994).
[26] G. Kresse and D. Joubert, Phys. Rev. B **59**, 1758 (1999).
[27] J. P. Perdew and A. Zunger, Phys. Rev. B **23**, 5048 (1981).
[28] A. Togo, F. Oba, and I. Tanaka, Phys. Rev. B **78**, 134106 (2008).
[29] Y. Wang, J. J. Wang, W. Y. Wang, Z. G. Mei, S. L. Shang, L. Q. Chen, and Z. K. Liu, J. Phys. Condens. Matter **22**, 202201 (2010).
[30] P. Lambin and J. P. Vigneron, Phys. Rev. B **29**, 3430 (1984).
[31] L. Lindsay, D. A. Broido, and T. L. Reinecke, Phys. Rev. B **87**, 165201 (2013).
[32] Ioffe Institute, http://www.ioffe.ru/SVA/NSM/Semicond/SiC/thermal.html.
[33] M. C. Gupta and J. Ballato, *The Handbook of Photonics*, 2nd ed. (CRC Press, Cleveland, 2006).
[34] S. R. Smith, A. O. Evwaraye, W. C. Mitchel, and M. A. Capano, J. Electron. Mater. **28**, 190 (1999).
[35] J. Isoya, T. Ohshima, N. Morishita, T. Kamiya, H. Itoh, and S. Yamasaki, J. Phys. B: Condens. Matter **340–342**, 903 (2003).
[36] A. Fukumoto, Phys. Rev. B **53**, 4458 (1996).
[37] F. Bechstedt, A. Fissel, J. Furthmüller, U. Grossner, and A. Zywietz, J. Phys. Condens. Matter **13**, 9027 (2001).

[38] T. T. Petrenko and T. L. Petrenko, Phys. Rev. B **93**, 165203 (2016).

[39] T. Oda, Y. Zhang, and W. J. Weber, J. Chem. Phys. **139**, 124707 (2013).

[40] A. Kundu, N. Mingo, D. A. Broido, and D. A. Stewart, Phys. Rev. B **84**, 125426 (2011).

[41] J. Garg, N. Bonini, B. Kozinsky, and N. Marzari, Phys. Rev. Lett. **106**, 045901 (2011).

[42] A. R. Oganov and V. L. Solozhenko, J. Superhard Mater. **31**, 285 (2009).

[43] M. Vlasse, G. A. Slack, M. Garbauskas, J. S. Kasper, and J. C. Viala, J. Solid State Chem. **63**, 31 (1986).

[44] T. L. Aselage, J. Mater. Res. **13**, 1786 (1998).

[45] N. A. Katcho, J. Carrete, W. Li, and N. Mingo, Phys. Rev. B **90**, 094117 (2014).

[46] E. Economou, in *Green's Function in Quantum Physics*, 2nd ed., edited by M. Cardona, P. Fulde, and H. J. Queisser (Springer, New York, 1983), pp. 108–109.

[47] V. Lordi, P. Erhart, and D. Åberg, Phys. Rev. B **81**, 235204 (2010).

[48] P. Erhart, D. Åberg, and V. Lordi, Phys. Rev. B **81**, 195216 (2010).

[49] H. Kuwabara, S. Shiokawa, and S. Yamada, Phys. Status Solidi A **16**, K67 (1973).

[50] S. H. Hagen and A. W. C. van Kemenade, Phys. Status Solidi A **33**, 97 (1976).

[51] T. Yang, X. Chang, J. Chen, K.-C. Chou, and X. Hou, Nanoscale **7**, 8955 (2015).

[52] Y. Yang, H. Yang, G. Wei, L. Wang, M. Shang, Z. Yang, B. Tang, and W. Yang, J. Mater. Chem. C **2**, 4515 (2014).

[53] B. S. Richards, A. Lambertz, R. P. Corkish, C. A. Zorman, M. Mehregany, M. Ionescu, and M. A. Green, *Proceedings of 3rd World Conference on Photovoltaic Energy Conversion, Osaka, 2003* (Arisumi Printing, Osaka, 2003), p. 2738.

[54] D. E. Onopko, A. I. Ryskin, and N. T. Bagraev, Semiconductors **30**, 82 (1996).